

Self-propulsion of a flapping flexible plate near the ground

Chao Tang, Haibo Huang, Peng Gao, and Xi-Yun Lu*

Department of Modern Mechanics, University of Science and Technology of China, Hefei, Anhui 230026, China

(Received 9 March 2016; revised manuscript received 11 July 2016; published 21 September 2016)

The self-propulsion of a three-dimensional flapping flexible plate near the ground is studied using an immersed boundary-lattice Boltzmann method for fluid flow and a finite-element method for plate motion. When the leading edge of the flexible plate is forced into a vertical oscillation near the ground, the entire plate moves freely due to the fluid-structure interaction. The mechanisms underlying the dynamics of the plate near the ground are elucidated. Based on the propulsive behaviors of the flapping plate, three distinct regimes due to the ground effect can be qualitatively identified. These regimes can be described briefly as the expensive, benefited, and uninfluenced propulsion regimes. The analysis of unsteady dynamics and plate deformation indicates that the ground effect becomes weaker for a more flexible plate. We have found that a suitable degree of flexibility can improve propulsion near the ground. The vortical structure around the plate and the pressure distribution on the plate are analyzed to understand propulsive behaviors. The results obtained in this study can provide some physical insights into the propulsive mechanisms of a flapping flexible plate near the ground.

DOI: [10.1103/PhysRevE.94.033113](https://doi.org/10.1103/PhysRevE.94.033113)

I. INTRODUCTION

Aquatic animals have developed a superior ability to swim in complex environments. Swimming near the ground can yield hydrodynamic benefits. The fins of aquatic creatures have complex behaviors that depend mainly on the internal distribution of compliant components. As a result, the propulsor of a swimming animal is usually flexible and can become deformed by motion [1–3]. The dynamics of a flapping flexible body near the ground and the mechanisms relevant to the unsteady ground effect remain unclear [4,5], and they are highly desirable topics of study due to their fundamental principles and potential applications.

Some work has been performed on a flapping wing near a solid boundary in order to understand the flying or swimming dynamics in the unsteady-ground effect. The ground effect on basic insect hovering was studied numerically [4], and similarly the ground effect on the dynamics of an oscillating airfoil was examined experimentally [6]. A three-dimensional (3D) model of a bird with unsteady flight patterns consisting of flapping, twisting, and folding motions near the ground was investigated numerically [7]. Because a stingray-inspired physical model was used to mimic undulatory swimmers, no significant benefits of near-ground swimming were identified [8]. A recent detailed study of an aerofoil undergoing pitch oscillations near the ground [9] indicated that the ground effect can enhance thrust for the pitching aerofoil. Furthermore, the hydrodynamic benefits of swimming near the ground for a heaving flexible plate were investigated experimentally in Ref. [5]. The results of that study indicated that the ground effect can suppress the 3D torsional mode of the plate, thereby increasing thrust and propulsive efficiency.

The wing and fin are usually flexible, and they can deform passively in response to fluid forces in their motion. Consequently, the role of flexibility in flapping propulsion has been investigated. The optimal flexibility of a flapping flexible body in an inviscid fluid was studied in terms of an analysis of the

motion of the flexible body with a vortex-sheet wake [10,11]. The influence of the bending rigidity of a flexible heaving wing on its propulsive performance was also investigated in the inviscid limit [12]. Recently, a small-amplitude theory was proposed to model a flapping wing that pitches passively due to a combination of wing compliance, inertia, and fluid forces [13]. Furthermore, some numerical investigations were carried out to reveal the effects of flexibility on propulsion [14–17]. In addition, experiments were performed to understand the role of wing and fin flexibility in flapping locomotion [18,19].

For animals in a steady state of free swimming, the mean thrust generated balances the resistance experienced by the surrounding fluid. Actually, the dynamics of a flow past a stationary object is different from that of a free-moving object in a stationary fluid [20]. Some efforts have been made to investigate the locomotion of flapping flexible foils or plates in a stationary fluid [21–26]. To our knowledge, however, there has been no relevant work on the free locomotion of a flexible plate near the ground. Thus, it is necessary to study the dynamical behaviors relevant to free motion near the ground.

In the present study, we consider a 3D flexible plate whose leading edge is forced to move sinusoidally near the ground in a stationary fluid. As a result of the fluid-structure interaction, the plate moves freely in the fluid subject to the ground effect. The ground effect on the propulsive properties, deformation, and motion of the plate, and the vortical structures around the plate, are investigated. The purpose of this study is to improve our understanding of the physical mechanisms relevant to the free locomotion of a flapping flexible plate near the ground.

This paper is organized as follows. The physical problem and its mathematical formulation are presented in Sec. II. The numerical method and validation are described in Sec. III. Detailed results are discussed in Sec. IV, and concluding remarks are presented in Sec. V.

II. PHYSICAL PROBLEM AND MATHEMATICAL FORMULATION

As shown in Fig. 1, we consider a flexible plate with length c and span length b that is placed in proximity to a planar

*xlu@ustc.edu.cn

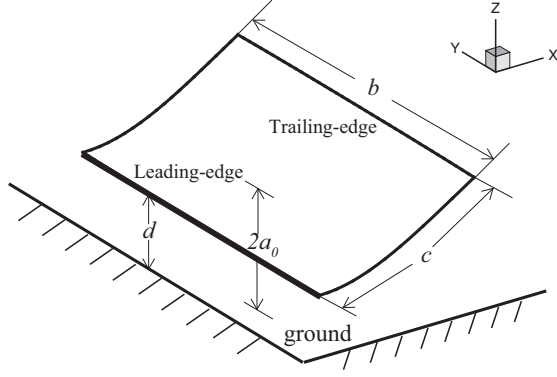


FIG. 1. Schematic of a flapping flexible plate near the ground.

ground. The surrounding fluid is stationary. The leading edge of the plate is forced to perform a vertical oscillation described as

$$a(t) = a_0 \cos(2\pi ft), \quad (1)$$

where a_0 and f are the oscillating amplitude and the frequency, respectively. The average distance between the leading edge of the plate and the ground is d . Here, a local moving

$$\rho_s h \frac{\partial^2 \mathbf{X}}{\partial t^2} = \sum_{i,j=1}^2 \left[\frac{\partial}{\partial s_i} \left\{ \varphi_{ij} \left[\delta_{ij} - \left(\frac{\partial \mathbf{X}}{\partial s_i} \cdot \frac{\partial \mathbf{X}}{\partial s_j} \right)^{-1/2} \right] \frac{\partial \mathbf{X}}{\partial s_j} - \frac{\partial}{\partial s_j} \left(\gamma_{ij} \frac{\partial^2 \mathbf{X}}{\partial s_i \partial s_j} \right) \right\} \right] + \mathbf{F}, \quad (4)$$

where \mathbf{X} is the position vector of the plate, \mathbf{F} is the Lagrangian force exerted on the plate by the fluid, and ρ_s and h are the mass density and the thickness of the plate. φ_{ij} is the in-plane effect matrix, where $\varphi_{11} = \varphi_{22} = Eh$ is the stretching stiffness and $\varphi_{12} = Gh$ is the shearing stiffness of the plate. γ_{ij} is the out-of-plane effect matrix, where $\gamma_{11} = \gamma_{22} = \gamma_{12} = EI$ is the bending stiffness of the plate. In addition, δ_{ij} is the Kronecker delta function.

The characteristic quantities ρ , f , and c are chosen to nondimensionalize the above equations and the computational domain. The dimensionless governing parameters are described as follows: the heaving amplitude $A = a_0/c$; the frequency Reynolds number $\text{Re}_f = \rho f c^2 / \mu$; the frequency ratio of the heaving frequency and the natural frequency, $F = f/f_n$, where $f_n = (1.8751^2 / 2\pi c^2) \sqrt{EI / \rho_s h}$ is the first chordwise natural frequency of plate using the Euler-Bernoulli beam theory; the stretching stiffness $S = Eh / \rho f^2 c^3$; the bending stiffness $K = EI / \rho f^2 c^5$; the mass ratio of the plate and the fluid, $M = \rho_s h / \rho c$; the aspect ratio of the plate, $H = b/c$; and the ground distance between the mean location of the leading edge of plate and the ground, $D = d/c$. Based on the definition of F , it can be changed by modifying the flexibility and thereby the natural frequency of the plate without varying f . In addition, we have examined the chordwise and spanwise deformation of the plate and identified that the spanwise deformation is small for the parameters considered in this study. Therefore, the natural frequency is defined only in terms of the first chordwise bending mode.

curvilinear coordinate system (s_1, s_2) defined on the plate surface is used to describe the configuration and motion of the plate.

As a result of the interplay of the plate elasticity, the leading-edge forcing, and the forces exerted by the surrounding fluid, the plate starts to move freely and passively in the stationary fluid. The active pitching angle is zero in this model, meaning that only the leading edge of the plate is restricted with its vertical motion being prescribed, while the remainder of the plate can move freely in the entire fluid domain.

To investigate this system of the fluid and flapping flexible plate interaction, the incompressible Navier-Stokes equations are used to simulate the fluid flow,

$$\frac{\partial \mathbf{v}}{\partial t} + \mathbf{v} \cdot \nabla \mathbf{v} = -\frac{1}{\rho} \nabla p + \frac{\mu}{\rho} \nabla^2 \mathbf{v} + \mathbf{f}, \quad (2)$$

$$\nabla \cdot \mathbf{v} = 0, \quad (3)$$

where \mathbf{v} is the velocity, p is the pressure, ρ is the density of the fluid, μ is the dynamic viscosity, and \mathbf{f} is the body force term. The structural equation is employed to describe the plate deformation and motion [26–28],

III. NUMERICAL METHOD AND VALIDATION

The governing equations of the fluid-plate problem are solved numerically using an immersed boundary-lattice Boltzmann method (IB-LBM) for the fluid flow and a finite-element method for the motion of the flexible plate. When the IB method is applied to treat flow-structure interaction [29,30], the body force term \mathbf{f} in Eq. (2) is used as an interaction force between the fluid and the immersed boundary to enforce the no-slip velocity boundary condition. The lattice Boltzmann equation with the body force model [31] and the nonuniform mesh technique [28] are employed to solve the viscous fluid flow. Equation (4) for the deformable plate is discretized by a finite-element method, and the deformation with a large displacement of the plate is handled by the corotational scheme [32]. A detailed description of the numerical method can be found in our previous papers [23,28].

Based on our convergence studies with different computational domains and lattice spacing, the computational domain for fluid flow is chosen as $[-10, 30] \times [-10, 10] \times [0, 15]$ in the x , y , and z directions. A nonuniform mesh technique is employed to improve computational efficiency. In the x direction, the mesh is uniform with spacing 0.025. In the y and z directions, the mesh is uniform with spacing 0.025 in the near region of the plate and gradually increases in a geometric progression to a coarse spacing 0.1 in the far boundary region. The time step is $\Delta t = 0.00025$ for the simulations of fluid flow and plate deformation, where the time is nondimensionalized by the oscillating period $T = 1/f$. Moreover, a finite moving computational domain [22,23] is used in the x direction to

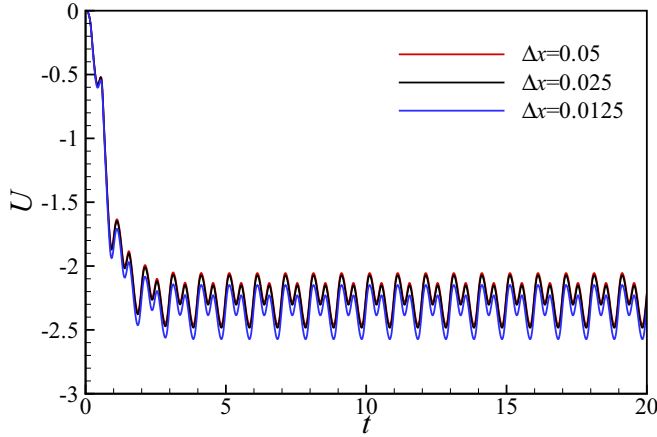


FIG. 2. Time-dependent propulsive velocity of a flapping flexible plate near the ground for three grid spacings with the parameters $D = 0.5$, $F = 0.6$, $H = 2.0$, $A = 0.25$, $M = 0.5$, and $Re_f = 100$.

allow the plate to move for a sufficiently long time. As the plate travels one lattice in the x direction, the computational domain is shifted, i.e., one layer is added at the inlet and another layer is removed at the outlet [22,23].

To assess the grid convergence in the present calculation, Fig. 2 shows the time-dependent propulsive velocity of a flapping flexible plate near the ground for different grid spacings. It is seen that the results for the grid spacing $\Delta x = 0.025$ and 0.0125 collapse together, indicating a reasonable grid convergence. Since the 3D calculation cost is high, we have chosen the grid spacing $\Delta x = 0.025$ in the present study.

Furthermore, to validate the present numerical method and its implementation, we consider a flapping flag in a uniform flow [27]. Figure 3 shows the time history of the lateral displacement of the lower corner on the trailing edge of the flag for the Reynolds numbers $Re = 100$ and 500 , where $Re = \rho c U_\infty / \mu$ with the uniform flow velocity U_∞ . It is seen that the present results agree well with the previous ones [27]. In addition, the numerical strategy used in this study has been validated previously and applied with success to a wide range of fluid-structure interactions, such as the flapping motion of

an inverted flexible plate [33], the dynamics of fluid flow over a circular flexible plate [28], the locomotion of a flapping flexible plate [23,26], and the vorticity dynamics of fluid flow over a flapping plate [34].

IV. RESULTS AND DISCUSSION

We present here some typical results on the self-propulsion of a flapping flexible plate near the ground. Motivated by measurements of [35–39] and experiments on [40,41] flapping-based animal locomotion, the governing parameters used in this study are chosen as follows: frequency ratio $F = 0.15–1.5$, ground distance $D = 0.45–2.5$, aspect ratio $H = 1–4$, frequency Reynolds number $Re_f = 100$, heaving amplitude $A = 0.25$, mass ratio $M = 0.5$, and stretching stiffness $S = 1000$. In the present study, we investigate mainly the propulsive behaviors relevant to the ground effect, plate flexibility, and the aspect ratio based on the selection of those parameters, which also play an important role in animal locomotion [1–3].

A. Propulsive behaviors in the ground effect

The propulsive behaviors in the ground effect are first investigated based on some typical results in Fig. 4. For comparison, the case without the ground effect is also considered, and is denoted briefly by $D = \infty$. Here, we mainly use the results of $H = 2$ to elucidate the propulsive behaviors. Figure 4(a) shows the dimensionless mean propulsive speed U for $D = 0.5$. As F increases, which is related to the plate becoming more flexible for a fixed heaving frequency, the speed U increases to the maximum at approximately $F = 0.6$ and then decreases gradually. Compared with the curve for $D = \infty$, the ground effect increases the propulsive speed for all plate aspect ratios considered. As a typical case, the net increment of propulsive speed due to the ground effect (i.e., ΔU) is demonstrated in Fig. 4(a) for $H = 2$, which decreases gradually with the increase of F .

To maintain the self-propulsion of the flapping plate, input work is required and computed as a time integral of the power P performed by the surface of the body on the surrounding fluid during one flapping period. Here the input work W for

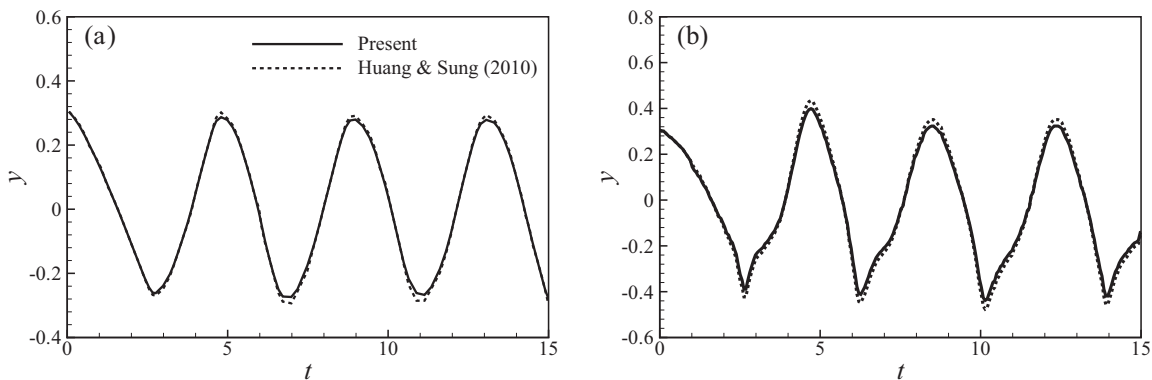


FIG. 3. Comparison of the present results and previous data [27] for the time history of the lateral displacement of the lower corner on the trailing edge of a flag with the parameters $H = 1.0$, $M = 1.0$, $K = 0.0001$, and $S = 1000$: (a) $Re = 100$ and (b) $Re = 500$.

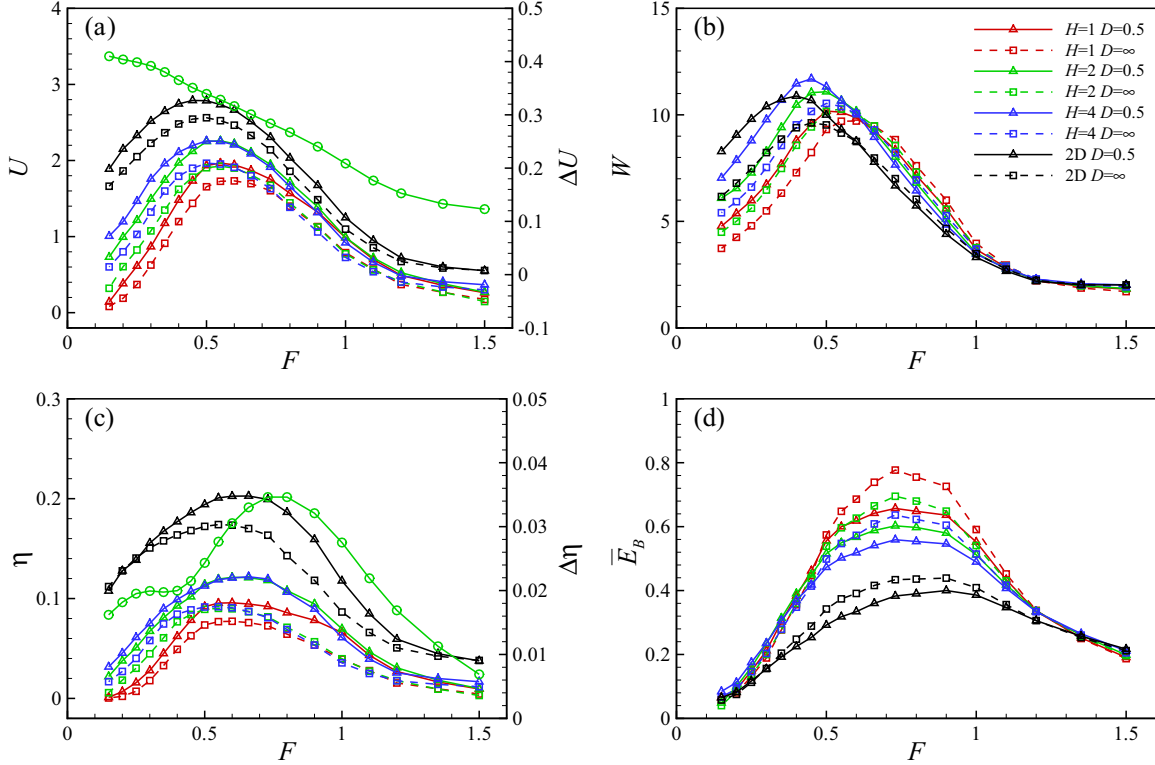


FIG. 4. Comparison of the metrics of propulsion with and without the ground effect: (a) mean propulsive speed, (b) input work during one period, (c) propulsive efficiency, and (d) mean bending energy for several aspect ratios and the 2D case. In (a) and (c), the line marked by circles represents the net increments of propulsive speed ΔU and propulsive efficiency $\Delta\eta$ for $H = 2$, respectively.

the unit area is expressed as

$$W = \int_{t_0}^{t_0+T} P dt = \frac{1}{H} \int_{t_0}^{t_0+T} \int_0^H \int_0^1 \mathbf{F}_r(s_1, s_2, t) \cdot \frac{\partial \mathbf{X}(s_1, s_2, t)}{\partial t} ds_1 ds_2 dt, \quad (5)$$

where \mathbf{F}_r represents the force on the surrounding fluid by the plate. From Fig. 4(b) for the input work W , it is noted that, compared with the $D = \infty$ case, more input work is needed for propulsion when $F < 0.5$ approximately, but somewhat less input work or no more input work is required when $0.5 < F < 1.0$. As F increases further or the plate becomes very flexible, the input work is nearly identical with and without the ground effect.

To characterize the propulsive efficiency of a self-propulsive body, the ratio of the kinetic energy of the body and the input work has been employed [22,23,42]. Therefore, the propulsive efficiency is represented as $\eta = \frac{1}{2} MU^2 / W$. It is seen from Fig. 4(c) that the ground effect can enhance the propulsive efficiency, which is more obvious when $0.5 < F < 1.0$, such as the net increment of propulsive efficiency $\Delta\eta$ for $H = 2$; this behavior is related to the fact that the propulsive speed is enhanced and the input work is somewhat decreased with respect to the $D = \infty$ case.

As the plate is flexible, it can store elastic potential energy because of the fluid-plate interaction. Note that the elastic potential due to the stretching effect is negligibly small based on our examination. Thus the elastic potential energy is

defined as

$$E_B(t) = \frac{K}{2} \int_0^H \int_0^1 \sum_{i,j=1}^2 \frac{\partial^2 \mathbf{X}}{\partial s_i^2} \cdot \frac{\partial^2 \mathbf{X}}{\partial s_j^2} ds_1 ds_2. \quad (6)$$

Then Fig. 4(d) shows the mean bending energy \bar{E}_B for the unit area in one flapping period. It is shown that the bending energy is less than that for the $D = \infty$ case when $0.5 < F < 1.0$, indicating that the ground assists in inhibiting the bending deformation of the plate. Furthermore, by means of the model for the frequency response of a rectangular cantilever beam immersed in a viscous fluid [43], we can redefine the frequency ratio using the frequency of the fluid-loaded plate, and we can identify with reasonable certainty that the elastic bending energy nearly corresponds to its maximum at this fluid-loaded plate resonance. In reality, the fundamental oscillation frequency of the plate in the viscous fluid lies in the range $O(10^0) - O(10^1)$ Hz, which mimics the animal flapping locomotion.

The effect of the aspect ratio of the plate on the propulsive behaviors is also analyzed in terms of the results in Fig. 4 for $H = 1, 2$, and 4. For comparison, the two-dimensional (2D) case is also calculated. It is seen from Figs. 4(a) and 4(c) that the propulsive speed and efficiency essentially increase with the aspect ratio, and the largest propulsive speed and efficiency occur for the 2D case. Moreover, the bending energy decreases as the aspect ratio increases, as shown in Fig. 4(d), indicating that the plate deformation is diminished.

Based on the results in Fig. 4 for several aspect ratios, we further analyze the propulsive behaviors of the flapping plate,

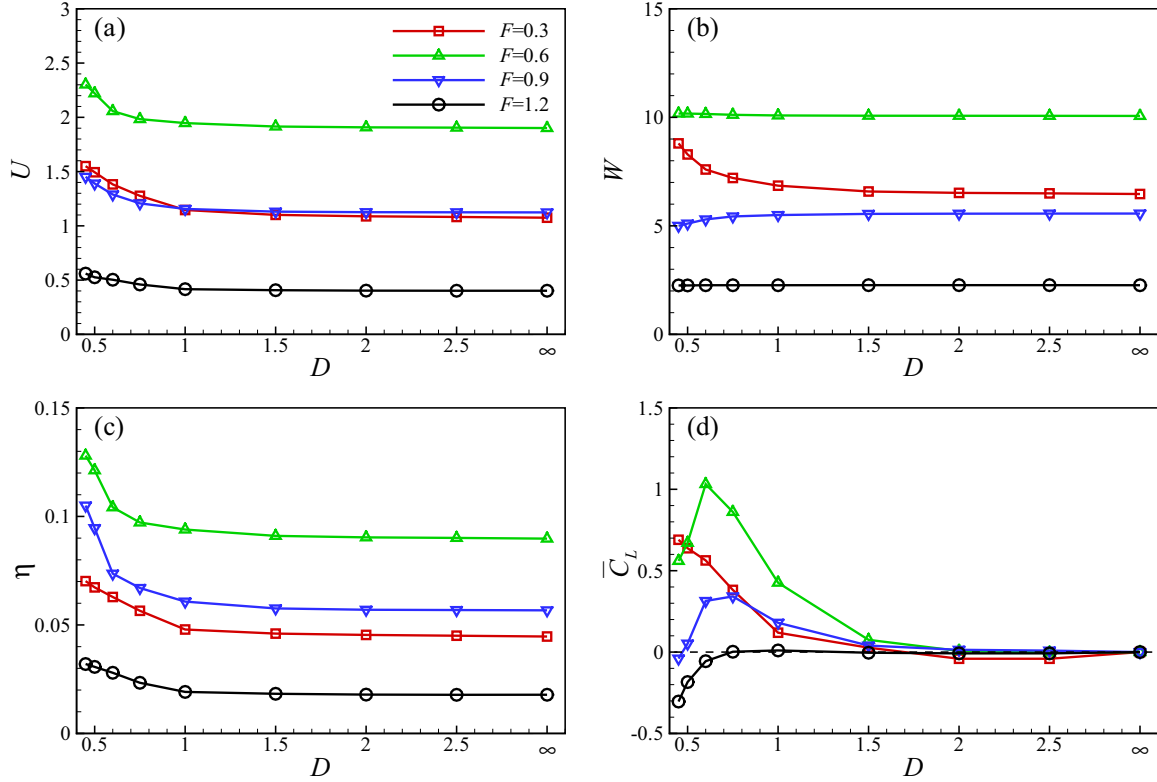


FIG. 5. The influence of ground proximity on the metrics of propulsion for $H = 2$: (a) mean propulsive speed, (b) input work in one flapping cycle, (c) propulsive efficiency, and (d) mean lift coefficient for several frequency ratios.

which can be briefly described as three distinct regimes due to the ground effect, i.e., expensive propulsion ($F < 0.5$), benefited propulsion ($0.5 < F < 1.0$), and uninfluenced propulsion ($F > 1.0$). Here, we further describe the qualitative distinction for these regimes. From Fig. 4(c), the net increment of propulsive efficiency is enlarged for approximately $0.5 < F < 1.0$. Moreover, less input work with respect to the $D = \infty$ case is required in Fig. 4(b) and less bending energy is generated in Fig. 4(d). Therefore, a suitable degree of flexibility, which is associated with the fluid-loaded plate resonance region under a forced heaving oscillation, can lead to significant propulsive benefits. In the expensive propulsion regime for $F < 0.5$, the propulsive speed due to the ground effect is increased, and a larger input work occurs for the flapping plate locomotion. In the uninfluenced propulsion regime for $F > 1.0$, the propulsive properties are nearly unchanged by the ground effect; therefore, no near-ground benefits are gained. In addition, we should indicate that the numerical bounds are classified approximately by F based on the results obtained in this study, which are not rigorous mathematically. The purpose of the classification of the three regimes is to clearly investigate the propulsive properties and physical mechanisms.

The influence of ground proximity on propulsive behaviors is investigated further. The propulsive speed and efficiency shown in Figs. 5(a) and 5(c) decrease monotonously as D increases, and they are nearly unchanged for $D > 1.5$, indicating that the ground effect becomes negligible. From Fig. 5(b), the input work W at the close ground proximity is associated with the frequency ratio F . As D decreases, it is interesting to note that W increases obviously for $F = 0.3$,

W decreases somewhat for $F = 0.6$ and 0.9 , and is nearly unchanged for $F = 1.2$. In addition, the thrust and power scaling analysis has been performed based on the inviscid theory for a pitching rigid airfoil near a solid boundary in a free-stream flow [9]. Therefore, it is worthwhile to try to perform a relevant scaling analysis in future work, even though the present case is more complex.

Because of the ground effect, a mean lift on the flexible plate is generated, which is closely associated with the vortical structures around the plate discussed below. As shown in Fig. 5(d), there exist different behaviors of the mean lift coefficient \overline{C}_L near the ground in three distinct regimes. The mean lift coefficient \overline{C}_L decreases with D and even becomes somewhat negative before approaching the $D = \infty$ case for $F = 0.3$. This behavior is consistent with the unsteady propulsion of a pitching rigid foil near the ground [9]. For $F = 0.6$ and 0.9 , \overline{C}_L first increases and then decreases to be even negative as D increases, and eventually it tends to vanish as D increases further. Moreover, \overline{C}_L is negative at the close ground proximity and tends to be zero with the increase of D for $F = 1.2$.

B. Unsteady dynamics and plate deformation

To understand the propulsive behaviors that occur in the ground effect, unsteady dynamics and plate deformation are investigated further. Figure 6 shows the time-dependent drag coefficient and input power in one flapping cycle for $F = 0.3$, 0.6 , and 1.2 , lying in the three distinct regimes, respectively. Note that, as the plate spontaneously propels itself by a

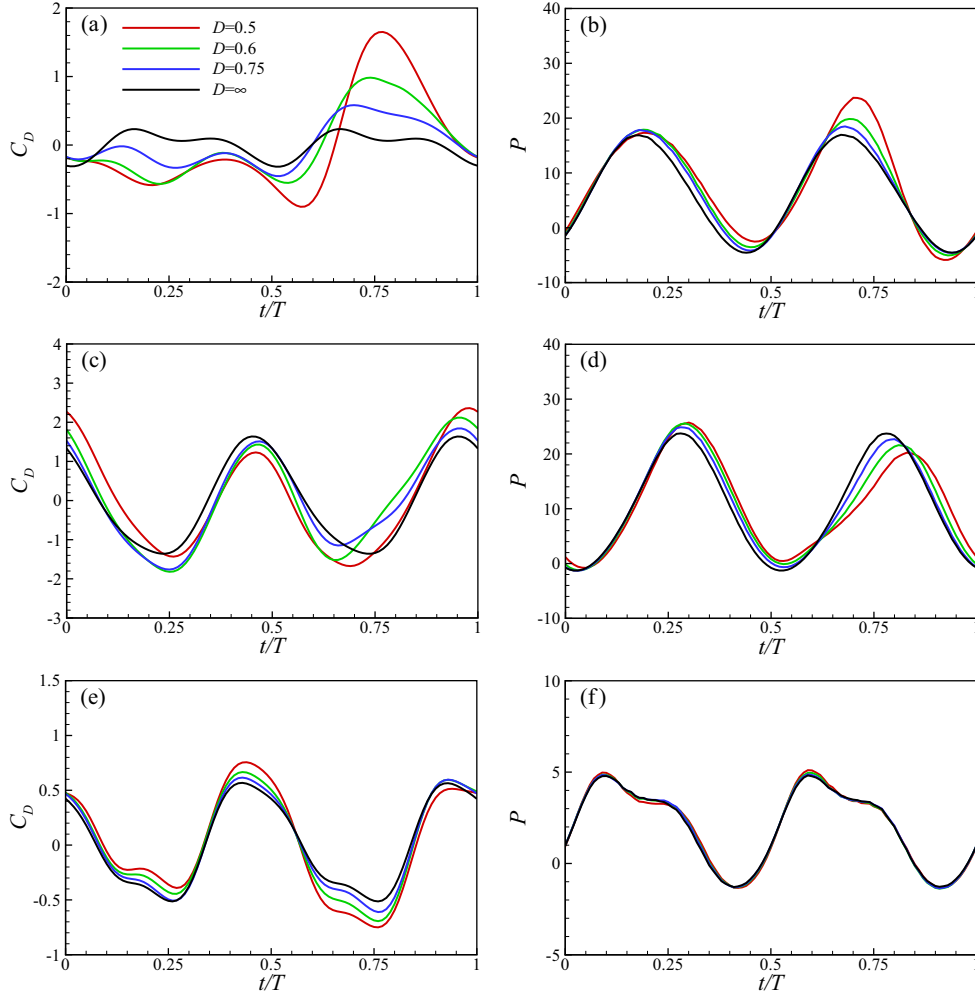


FIG. 6. Time-dependent drag force (left column) and input power (right column) in one flapping cycle for $H = 2$: (a,b) $F = 0.3$; (c,d) 0.6; and (e,f) 1.2.

constant mean velocity, the mean drag or thrust is zero over one flapping cycle, even though time-dependent variations occur. According to the leading-edge oscillation in Eq. (1), the first and second half-cycles correspond to the leading edge of the plate toward the ground and away from the ground, respectively, and they can be described briefly as a downstroke and an upstroke. The behaviors of the dynamics and the deformation will be analyzed below.

As shown in Fig. 6(a) for $F = 0.3$, thrust or negative drag is generated over the downstroke, and drag is formed in some part of the upstroke. Compared with the profiles for different ground distances, the mean thrust in the downstroke decreases as D increases. For $D = \infty$, the curves of C_D both in the downstroke and the upstroke are consistent with each other, and the corresponding mean values vanish. With the increase of F , as shown in Fig. 6(c) for $F = 0.6$, the profiles of drag are essentially similar to each other both in the downstroke and the upstroke, even though somewhat of a difference occurs for different ground distances. Moreover, it is shown that the mean thrust in the upstroke is generated, as shown in Fig. 6(e) for $F = 1.2$.

Furthermore, as shown in Fig. 6(b) for $F = 0.3$, an obvious increase in the input power is observed in the upstroke as

D decreases. This is consistent with the results in Fig. 4(b), which show that more input work due to the ground effect is needed when the plate is stiff enough. As shown in Fig. 6(d) for $F = 0.6$, with the decrease of D , the input power decreases in the period $0.6 < t/T < 0.8$. Thus the total input work in one period shows a slight decrease in the ground effect of approximately $0.5 < F < 1.0$, as shown in Fig. 4(b). From Fig. 6(f) for $F = 1.2$, the profiles of the input power with and without the ground effect nearly collapse, indicating that the ground effect becomes very weak. Moreover, as the chordwise bending mode takes a dominant role in the plate deformation, there exist similar behaviors for the several aspect ratios considered here.

The dynamics of the flapping flexible plate is associated with its deformation. Figure 7 shows the plate deformation shapes at several instances during one flapping cycle with and without the ground effect for $F = 0.6$. From $t/T = 0$ to 0.375 in the downstroke, the plate shapes for $D = 0.5$ and ∞ collapse nearly together. Then, from $t/T = 0.5$ to 0.875 in the upstroke, the plate demonstrates different shapes for $D = 0.5$ and ∞ . It is seen that the plate deformation is obviously suppressed by the ground at $t/T = 0.5$ to 0.625 when the flapping plate is near the ground. This behavior is consistent

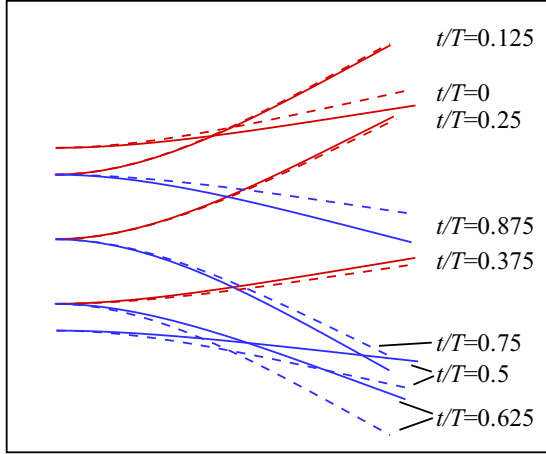


FIG. 7. Plate deformation shape on the spanwise symmetry plane at eight instances during one flapping cycle with and without the ground effect for $F = 0.6$ and $H = 2.0$. The solid and dashed lines represent the shapes at $D = 0.5$ and ∞ , respectively. The red and blue lines correspond to the downstroke and upstroke period.

with the experimental finding [5] that the ground effect can suppress the torsional mode of the plate, thereby increasing propulsive efficiency, as shown in Fig. 4.

Furthermore, Fig. 8 shows the vertical displacement of the midpoint on the trailing edge (z_t) and bending energy (E_B) of the plate with and without the ground effect. It is seen from Fig. 8(a) that the phase shift of z_t with respect to the forced oscillation of the leading edge increases as F increases. Comparing the time histories of z_t for $D = 0.5$ and ∞ , an obvious difference occurs for $F = 0.6$, and the curves are virtually coincident for $F = 0.3$ and 1.2 . The plate deformation is related to the pressure distribution on the plate, which will be discussed below.

The time-dependent bending energy E_B is also shown in Fig. 8(b). The larger amplitude of E_B is formed for $F = 0.6$, which is reasonably consistent with the larger vertical displacement z_t in Fig. 8(a). Moreover, the difference in bending energy between $D = 0.5$ and ∞ mainly occurs in the upstroke. The bending energy has a smaller amplitude for $F = 0.3$ and a larger amplitude for $F = 0.6$. When the plate becomes more flexible, e.g., $F = 1.2$ in Fig. 8, the deformation

and the bending energy of the plate are nearly identical for $D = 0.5$ and ∞ , consistent with the input power in Fig. 6(f). This behavior indicates that the ground effect becomes weaker for a more flexible plate.

C. Vortical structure and pressure distribution

The propulsive behaviors of a flapping flexible plate are closely associated with vortical structures [34,44]. Based on an analysis of vorticity dynamics, the force and input work of a flapping plate are dominated by the attached vorticity and the local vortical structure close to the plate [34]. Thus we discuss further the vortical structures around the plate and the pressure distribution on the plate in the benefited propulsion regime, and we analyze their connection with the metrics of propulsion shown above.

Figure 9 shows the vortical structures depicted by the isosurface of the Q criterion [45] and the spanwise vorticity contours at four instants during one flapping cycle for $F = 0.6$. It is seen that the wake behind the flapping plate consists of two sets of complex-shaped vortical structures. Because of the ground effect, the vortical structures along the upper and lower sets are no longer symmetric in the wake, resulting in the generation of mean lift about $\bar{C}_L = 0.55$, as shown in Fig. 5(d). Based on the evolution of the 3D vortical structures, it is shown that the vortices that were shed from the trailing edge of the plate connect with those from the two side-edges to essentially form the hairpin-like vortical structures in the upper set. The pattern of vortical structures is similar to the counterpart for the $D = \infty$ case. The vortical structures in the lower set interact with the ground to induce vorticity on the ground, and they evolve as the ringlike vortical structures near the ground. Moreover, based on the spanwise vorticity contours in the spanwise symmetry plane, the vortices that were shed from the plate are clearly observed, and the concentrated vorticity is induced on the ground.

We investigate further the connection between the vortical structures and the forces on the plate. Figure 10 shows the distribution of pressure coefficient C_p on the spanwise symmetry plane corresponding to the four instances in Fig. 9, where $C_p = (p - p_\infty) / \frac{1}{2} \rho f^2 c^2$. For comparison, the pressure distributions with and without the ground effect are presented. As shown in Fig. 10(a) at $t/T = 0$, the enclosed area of the

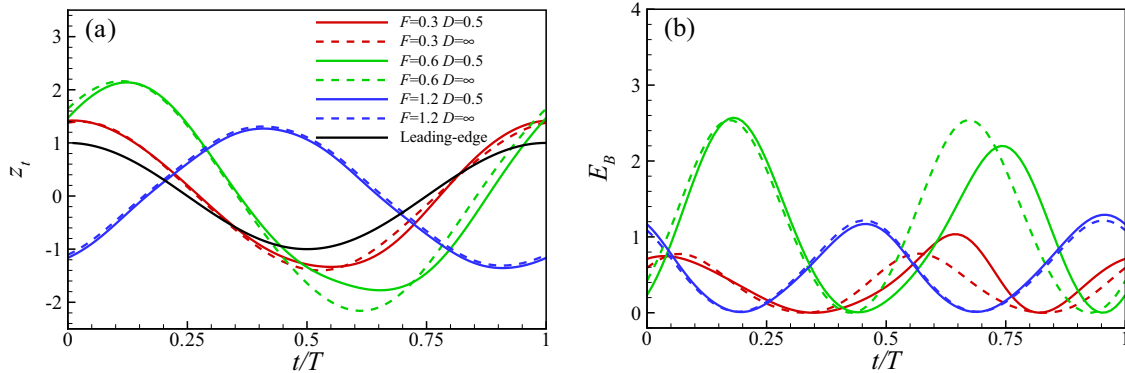


FIG. 8. Time-dependent deformation and bending energy during one flapping cycle for $H = 2$: (a) vertical displacement of the midpoint on the trailing edge; (b) bending energy.

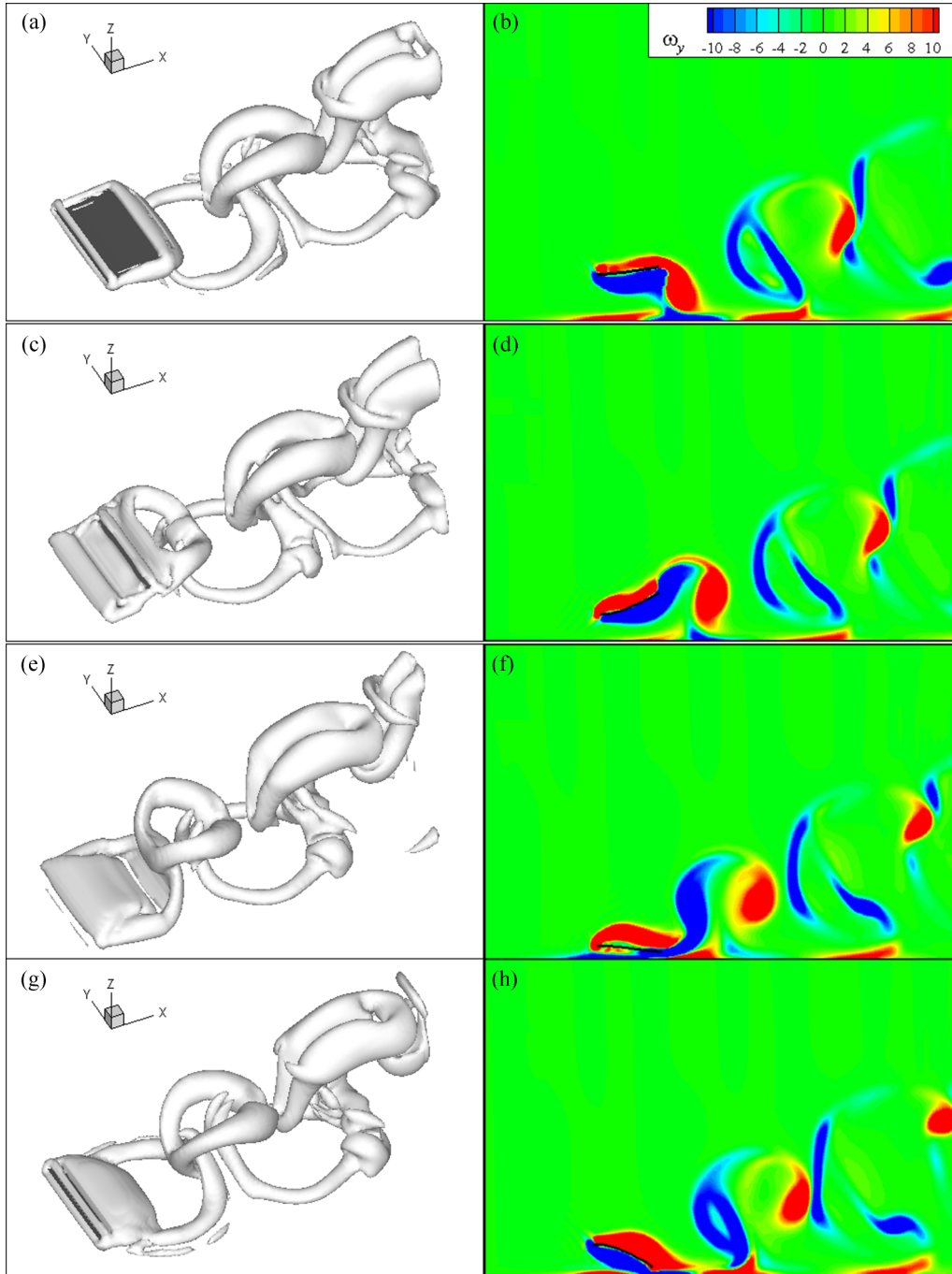


FIG. 9. Vortical structures visualized by an isosurface of the Q criterion with $Q = 1$ (left column) and spanwise vorticity contours on the spanwise symmetry plane (right column) during one flapping cycle for $F = 0.6$, $H = 2$, and $D = 0.5$: (a,b) $t/T = 0$, (c,d) 0.25, (e,f) 0.5, and (g,h) 0.75.

pressure curves for $D = 0.5$ is enlarged with respect to the $D = \infty$ case. This means that the force on the plate due to the pressure is enhanced by the ground effect. The vorticity patterns in Figs. 9(a) and 9(b) show that when the leading edge moves upward to its maximum location, stronger vorticity is generated on the lower side of the plate, inducing a stronger suction force with a lower pressure distribution in Fig. 10(a), and weaker vorticity is formed on the upper side with a somewhat higher pressure distribution in Fig. 10(a).

Then, as the plate moves downward, the pressure distributions in Fig. 10(b) and the plate shapes in Fig. 7 at $t/T = 0.25$ are similar to each other for the $D = 0.5$ and ∞ cases. A higher upward lateral force is generated, which is mainly related to the circulatory force [5,46] at $t/T = 0.25$ with the largest instantaneous velocity of the leading edge. It is seen from Figs. 9(c) and 9(d) that the vortices are generated from the leading and trailing edges and the two side-edges of the plate. Since those attached vortices play a dominant role in

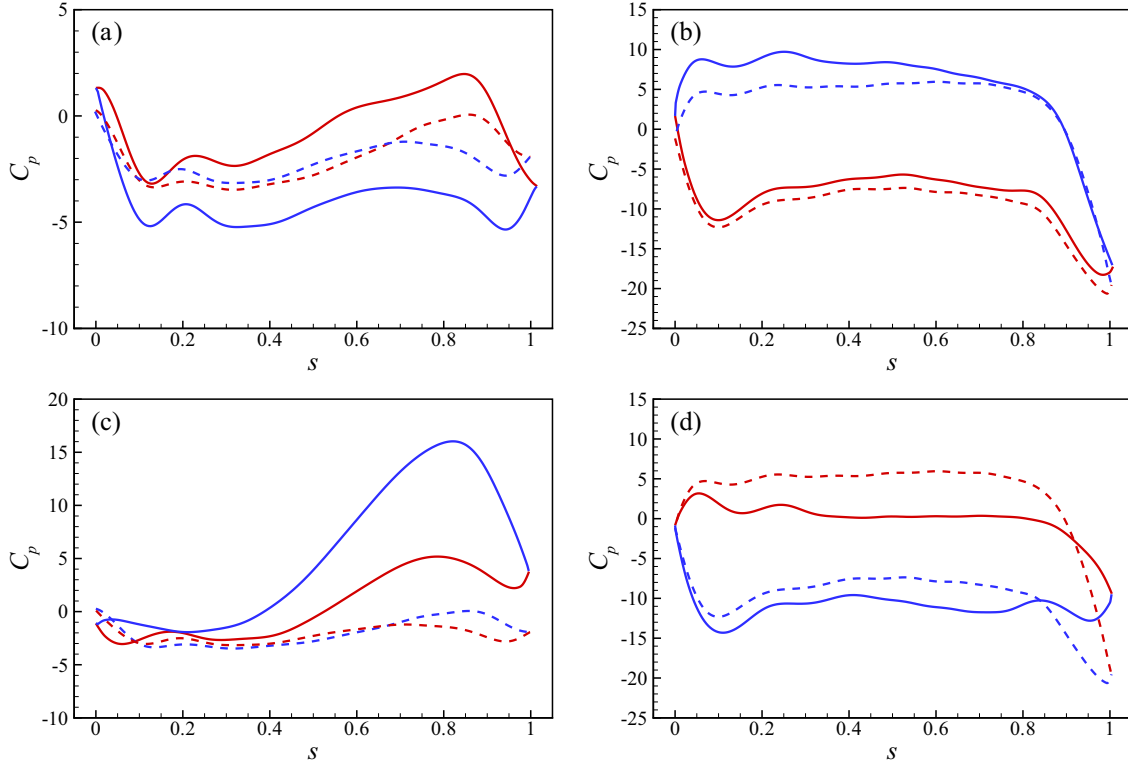


FIG. 10. Pressure distribution along the two side surfaces of a plate on the spanwise symmetry plane during one flapping cycle for $F = 0.6$, $H = 2$, and $D = 0.5$ and ∞ : (a) $t/T = 0$, (b) 0.25, (c) 0.5, and (d) 0.75. Here, the solid and dashed lines denote the results for $D = 0.5$ and ∞ , respectively, and the red and blue lines represent the distribution on the upper and lower surface of the plate.

the formation of forces on the plate [34], the forces are thus enhanced.

When the leading edge oscillates to the nearest location away from the ground at $t/T = 0.5$, the pressure distributions in Fig. 10(c) are enhanced due to the ground effect, particularly the pressure distribution on the lower side of the plate, which is similar to the lift enhancement of a lifting surface moving on solid ground [47]. The plate deformation is also suppressed by the ground, as shown in Fig. 7. The relevant mechanism can be understood from the analysis of vorticity dynamics. As shown in Figs. 9(e) and 9(f), a stronger leading-edge vortex is generated on the upper side of the plate, where a higher pressure distribution is induced. In the meantime, the attached trailing-edge vortex with a half-ring-like structure moves up due to the ground effect, and it interacts with the nearest downstream vortex ring in Fig. 9(e). Moreover, from the vorticity pattern of the gap flow between the plate and the ground in Fig. 9(f), it is seen that the positive and negative vortices are generated on the ground. This behavior is associated with a column jetlike flow induced by the plate's impact on the ground [48,49] when the plate moves toward the ground. Thus a reaction effect results in a higher pressure distribution on the lower side of the plate, which is much higher than the counterpart for the $D = \infty$ case as shown in Fig. 10(c).

As the plate moves upward at $t/T = 0.75$, the pressure distributions are shown in Fig. 10(d). An obvious difference in the pressure distributions for $D = 0.5$ and ∞ occurs in the trailing-edge region of the plate. It is seen from Figs. 9(g) and 9(h) that the vortices that were shed from the trailing

edge are obviously diminished since the trailing edge is near the ground, resulting in a smooth pressure distribution in the trailing-edge region. This behavior is also consistent with the lower bending energy with respect to the $D = \infty$ case at $t/T = 0.75$ in Fig. 8(b).

Finally, we analyze the relationship between the pressure distribution shown in Fig. 10 and the metrics of propulsion for $F = 0.6$. Since the pressure difference across the plate is relatively weak at $t/T = 0$, the force on the plate due to the pressure is small. As the leading edge of the plate moves downward, a higher pressure distribution on the lower side of the plate and a lower pressure distribution on the upper side are formed, as shown in Fig. 10(b). Because a larger lift force is generated, a higher input power is required for the flapping plate locomotion. Thus the input power nearly reaches a maximum around $t/T = 0.25$ in Fig. 6(d). When the leading edge reaches the lowest position at $t/T = 0.5$, a higher pressure region is observed between the rear part of the plate and the ground, as shown in Fig. 10(c), which suppresses the deformation of the plate as shown in Fig. 8 when the plate moves upward. As the leading edge moves upward, a lower pressure distribution on the lower side of the plate is formed at $t/T = 0.75$, resulting in a higher input power required to overcome the force due to the pressure, as shown in Fig. 6(d).

V. CONCLUDING REMARKS

We have studied the self-propulsion of a flapping flexible plate near the ground. Numerous simulations were performed

for a wide range of parameters, and various mechanisms governing the dynamics of the plate were investigated. Here we summarize the results that are relevant to the self-propulsion of the plate.

Based on the investigation of the propulsive behaviors of a flapping plate, three distinct regimes due to the ground effect can be qualitatively identified: expensive, benefited, and uninfluenced propulsion regime. The qualitative distinction for these regimes is presented as follows. In the benefited regime, the net increment of propulsive efficiency is increased for approximately $0.5 < F < 1.0$, with less input work and less bending deformation with respect to the $D = \infty$ case. In the expensive propulsion regime for $F < 0.5$, the propulsive speed near the ground is increased, and a larger amount of input work is required for plate locomotion. In the uninfluenced propulsion regime for $F > 1.0$, the propulsive properties are unchanged by the ground effect; therefore, no near-ground benefits are gained.

An analysis of the effect of ground proximity on propulsive properties indicates that propulsive speed and efficiency are

essentially enhanced near the ground. The three regimes have different properties with regard to input work and mean lift near the ground. Furthermore, the unsteady dynamics and deformation of a plate are investigated, and the behaviors of thrust and input power during downstroke and upstroke are also elucidated. We have found that a suitable degree of flexibility, which corresponds reasonably well to the fluid-loaded plate resonance region under a forced heaving oscillation, can improve propulsion near the ground. Finally, we have analyzed the vortical structures around the plate and the pressure distribution on the plate as well as their connection to the metrics of propulsion, as this helps us to understand the physical mechanisms of the self-propulsion of a flapping flexible plate near the ground.

ACKNOWLEDGMENTS

This work was supported by the National Natural Science Foundation of China (Grants No. 11372304 and No. 11621202) and by “Science Challenging Program”.

-
- [1] R. W. Blake, *Fish Locomotion* (Cambridge University Press, Cambridge, 1983).
 - [2] J. J. Videler, *Fish Swimming* (Chapman and Hall, New York, 1993).
 - [3] F. Fish and G. Lauder, *Annu. Rev. Fluid Mech.* **38**, 193 (2006).
 - [4] T. Gao and X.-Y. Lu, *Phys. Fluids* **20**, 087101 (2008).
 - [5] D. B. Quinn, G. V. Lauder, and A. J. Smits, *Bioinspir. Biomim.* **9**, 036008 (2014).
 - [6] H. Lu, K. B. Lua, T. T. Lim, and K. S. Yeo, *Exp. Fluids* **55**, 1787 (2014).
 - [7] J.-Y. Su, J.-H. Tang, C.-H. Wang, and J.-T. Yang, *Phys. Fluids* **25**, 093101 (2013).
 - [8] E. Blevins and G. V. Lauder, *Bioinspir. Biomim.* **8**, 016005 (2013).
 - [9] D. B. Quinn, K. W. Moored, P. A. Dewey, and A. J. Smits, *J. Fluid Mech.* **742**, 152 (2014).
 - [10] S. Alben, *J. Fluid Mech.* **614**, 355 (2008).
 - [11] S. Alben, C. Witt, T. V. Baker, E. Anderson, and G. V. Lauder, *Phys. Fluids* **24**, 051901 (2012).
 - [12] S. Michelin and S. G. Llewellyn Smith, *Phys. Fluids* **21**, 071902 (2009).
 - [13] M. N. J. Moore, *J. Fluid Mech.* **757**, 599 (2014).
 - [14] H. Masoud and A. Alexeev, *Phys. Rev. E* **81**, 056304 (2010).
 - [15] C.-K. Kang, H. Aono, C. E. S. Cesnik, and W. Shyy, *J. Fluid Mech.* **689**, 32 (2011).
 - [16] H. Dai, H. Luo, and J. F. Doyle, *J. Fluid Mech.* **693**, 473 (2012).
 - [17] R. Han, J. Zhang, L. Cao, and X.-Y. Lu, *J. Hydrodyn.* **27**, 496 (2015).
 - [18] S. E. Spagnolie, L. Moret, M. J. Shelley, and J. Zhang, *Phys. Fluids* **22**, 041903 (2010).
 - [19] P. A. Dewey, B. M. Boschitsch, K. W. Moored, H. A. Stone, and A. J. Smits, *J. Fluid Mech.* **732**, 29 (2013).
 - [20] T. Y.-T. Wu, *Adv. Appl. Mech.* **38**, 291 (2001).
 - [21] E. D. Tytell, C. Y. Hsu, T. L. Williams, A. H. Cohen, and L. J. Fauci, *Proc. Natl. Acad. Sci. USA* **107**, 19832 (2010).
 - [22] J. Zhang, N.-S. Liu, and X.-Y. Lu, *J. Fluid Mech.* **659**, 43 (2010).
 - [23] R.-N. Hua, L. Zhu, and X.-Y. Lu, *Phys. Fluids* **25**, 121901 (2013).
 - [24] Y.-L. Yu, *J. Fluid Mech.* **744**, 310 (2014).
 - [25] J. Hu and Q. Xiao, *J. Fluids Struct.* **46**, 77 (2014).
 - [26] C. Tang and X.-Y. Lu, *J. Hydrodyn.* **28**, 1 (2016).
 - [27] W.-X. Huang and H. J. Sung, *J. Fluid Mech.* **653**, 301 (2010).
 - [28] R.-N. Hua, L. Zhu, and X.-Y. Lu, *J. Fluid Mech.* **759**, 56 (2014).
 - [29] C. S. Peskin, *Acta Numer.* **11**, 479 (2002).
 - [30] R. Mittal and G. Iaccarino, *Annu. Rev. Fluid Mech.* **37**, 239 (2005).
 - [31] S. Chen and G. Doolen, *Annu. Rev. Fluid Mech.* **30**, 329 (1998).
 - [32] J. F. Doyle, *Nonlinear Analysis of Thin-Walled Structures: Statics, Dynamics, and Stability* (Springer-Verlag, New York, 2001).
 - [33] C. Tang, N.-S. Liu, and X.-Y. Lu, *Phys. Fluids* **27**, 073601 (2015).
 - [34] G.-J. Li and X.-Y. Lu, *J. Fluid Mech.* **712**, 598 (2012).
 - [35] R. Bainbridge, *J. Exp. Biol.* **35**, 109 (1958).
 - [36] F. E. Fish, *J. Exp. Biol.* **185**, 179 (1993).
 - [37] A. P. Willmott and C. P. Ellington, *J. Exp. Biol.* **200**, 2705 (1997).
 - [38] S. A. Combes and T. L. Daniel, *J. Exp. Biol.* **206**, 2979 (2003).
 - [39] S. A. Combes and T. L. Daniel, *J. Exp. Biol.* **206**, 2999 (2003).
 - [40] B. Thiria and R. Godoy-Diana, *Phys. Rev. E* **82**, 015303(R) (2010).
 - [41] S. Ramanarivo, R. Godoy-Diana, and B. Thiria, *Proc. Natl. Acad. Sci. USA* **108**, 5964 (2011).

- [42] S. Kern and P. Koumoutsakos, *J. Exp. Biol.* **209**, 4841 (2006).
- [43] C. A. Van Eysden and J. E. Sader, *J. Appl. Phys.* **101**, 044908 (2007).
- [44] H. Dong, R. Mittal, and F. M. Najjar, *J. Fluid Mech.* **566**, 309 (2006).
- [45] J. Jeong and F. Hussain, *J. Fluid Mech.* **285**, 69 (1995).
- [46] J. Katz and A. Plotkin, *Low-Speed Aerodynamics* (Cambridge University Press, Cambridge, 2001).
- [47] K. V. Rozhdestvensky, *Prog. Aerospace Sci.* **42**, 211 (2006).
- [48] P. Orlandi and R. Verzicco, *J. Fluid Mech.* **256**, 615 (1993).
- [49] C. C. Chu, C. T. Wang, and C. C. Chang, *Phys. Fluids* **7**, 1391 (1995).